Research Article | Vol. 25, No. 22 | 30 Oct 2017 | OPTICS EXPRESS 27506
Optics EXPRESS

Streaking of 43-attosecond soft-X-ray pulses generated by a passively CEP-stable mid-infrared driver

THOMAS GAUMNITZ, AROHI JAIN, YOANN PERTOT, MARTIN HUPPERT, INGA JORDAN, FERNANDO ARDANA-LAMAS, AND HANS JAKOB WÖRNER *

Laboratorium für Physikalische Chemie, ETH Zürich, Vladimir-Prelog-Weg 2, 8093 Zürich, Switzerland
**hwoerner@ethz.ch*

Abstract: Attosecond metrology has so far largely remained limited to titanium:sapphire lasers combined with an active stabilization of the carrier-envelope phase (CEP). These sources limit the achievable photon energy to ~100 eV which is too low to access X-ray absorption edges of most second- and third-row elements which are central to chemistry, biology and material science. Therefore, intense efforts are underway to extend attosecond metrology to the soft-X-ray (SXR) domain using mid-infrared (mid-IR) drivers. Here, we introduce and experimentally demonstrate a method that solves the long-standing problem of the complete temporal characterization of ultra-broadband (≫10 eV) attosecond pulses. We generalize the recently proposed Volkov-transform generalized projection algorithm (VTGPA) to the case of multiple overlapping photoelectron spectra and demonstrate its application to isolated attosecond pulses. This new approach overcomes all key limitations of previous attosecond-pulse reconstruction methods, in particular the central-momentum approximation (CMA), and it incorporates the physical, complex-valued and energy-dependent photoionization matrix elements. These properties make our approach general and particularly suitable for attosecond supercontinua of arbitrary bandwidth. We apply this method to attosecond SXR pulses generated from a two-cycle mid-IR driver, covering a bandwidth of ~100 eV and reaching photon energies up to 180 eV. We extract an SXR pulse duration of (43±1) as from our streaking measurements, defining a new world record. Our results prove that the popular and broadly available scheme of post-compressing the output of white-light-seeded optical parametric amplifiers is adequate to produce high-contrast isolated attosecond pulses covering the L-edges of silicon, phosphorous and sulfur. Our new reconstruction method and experimental results open the path to the production and characterization of attosecond pulses lasting less than one atomic unit of time (24 as) and covering X-ray absorption edges of most light elements.

OCIS codes: (320.7100) Ultrafast measurements; (140.7240) UV, EUV, and X-ray lasers; (320.6629) Supercontinuum generation.

References and links

1. G. Sansone, F. Kelkensberg, J. F. Pérez-Torres, F. Morales, M. F. Kling, W. Siu, O. Ghafur, P. Johnsson, M. Swoboda, E. Benedetti, F. Ferrari, F. Lépine, J. L. Sanz-Vicario, S. Zherebtsov, I. Znakovskaya, A. L'Huillier, M. Y. Ivanov, M. Nisoli, F. Martín, and M. J. J. Vrakking, "Electron localization following attosecond molecular photoionization," Nature **465**, 763–766 (2010).
2. F. Calegari, D. Ayuso, A. Trabattoni, L. Belshaw, S. De Camillis, S. Anumula, F. Frassetto, L. Poletto, A. Palacios, P. Decleva, J. B. Greenwood, F. Martìn, and M. Nisoli, "Ultrafast electron dynamics in phenylalanine initiated by attosecond pulses," Science **346**, 336–339 (2014).
3. P. M. Kraus, B. Mignolet, D. Baykusheva, A. Rupenyan, L. Horný, E. F. Penka, G. Grassi, O. I. Tolstikhin, J. Schneider, F. Jensen, L. B. Madsen, A. D. Bandrauk, F. Remacle, and H. J. Wörner, "Measurement and laser control of attosecond charge migration in ionized iodoacetylene," Science **350**, 790–795 (2015).
4. J. A. van Bokhoven and C. Lamberti, eds., *X-Ray Absorption and X-Ray Emission Spectroscopy: Theory and Applications* (John Wiley & Sons, 2016).
5. S. R. Leone, C. W. McCurdy, J. Burgdorfer, L. S. Cederbaum, Z. Chang, N. Dudovich, J. Feist, C. H. Greene, M. Ivanov, R. Kienberger, U. Keller, M. F. Kling, Z.-H. Loh, T. Pfeifer, A. N. Pfeiffer, R. Santra, K. Schafer, A. Stolow,

#305125 https://doi.org/10.1364/OE.25.027506
Journal © 2017 Received 21 Aug 2017; revised 8 Oct 2017; accepted 9 Oct 2017; published 24 Oct 2017

Optics EXPRESS

U. Thumm, and M. J. J. Vrakking, "What will it take to observe processes in 'real time'?" Nat. Photon. **8**, 162–166 (2014).
6. Y. Pertot, C. Schmidt, M. Matthews, A. Chauvet, M. Huppert, V. Svoboda, A. von Conta, A. Tehlar, D. Baykusheva, J.-P. Wolf, and H. J. Wörner, "Time-resolved X-ray absorption spectroscopy with a water window high-harmonic source," Science **355**, 264–267 (2017).
7. M. Hentschel, R. Kienberger, C. Spielmann, G. A. Reider, N. Milosevic, T. Brabec, P. Corkum, U. Heinzmann, M. Drescher, and F. Krausz, "Attosecond metrology," Nature **414**, 509–513 (2001).
8. P. M. Paul, E. S. Toma, P. Breger, G. Mullot, F. Augé, P. Balcou, H. G. Muller, and P. Agostini, "Observation of a train of attosecond pulses from high harmonic generation," Science **292**, 1689 (2001).
9. R. Kienberger, E. Goulielmakis, M. Uiberacker, A. Baltuska, V. Yakovlev, F. Bammer, A. Scrinzi, T. Westerwalbesloh, U. Kleineberg, U. Heinzmann, M. Drescher, and F. Krausz, "Atomic transient recorder," Nature **427**, 817–821 (2004).
10. G. Sansone, E. Benedetti, F. Calegari, C. Vozzi, L. Avaldi, R. Flammini, L. Poletto, P. Villoresi, C. Altucci, R. Velotta, S. Stagira, S. D. Silvestri, and M. Nisoli, "Isolated single-cycle attosecond pulses," Science **314**, 443 (2006).
11. G. Sansone, L. Poletto, and M. Nisoli, "High-energy attosecond light sources," Nat. Photon. **5**, 655–663 (2011).
12. K. Zhao, Q. Zhang, M. Chini, Y. Wu, X. Wang, and Z. Chang, "Tailoring a 67 attosecond pulse through advantageous phase-mismatch," Opt. Lett. **37**, 3891–3893 (2012).
13. M. Chini, K. Zhao, and Z. Chang, "The generation, characterization and applications of broadband isolated attosecond pulses," Nat. Photon. **8**, 178–186 (2014).
14. P. Colosimo, G. Doumy, C. I. Blaga, J. Wheeler, C. Hauri, F. Catoire, J. Tate, R. Chirla, A. M. March, G. G. Paulus, H. G. Muller, P. Agostini, and L. F. Dimauro, "Scaling strong-field interactions towards the classical limit," Nat. Phys. **4**, 386 (2008).
15. C. Vozzi, F. Calegari, E. Benedetti, S. Gasilov, G. Sansone, G. Cerullo, M. Nisoli, S. De Silvestri, and S. Stagira, "Millijoule-level phase-stabilized few-optical-cycle infrared parametric source," Opt. Lett. **32**, 2957–2959 (2007).
16. M.-C. Chen, P. Arpin, T. Popmintchev, M. Gerrity, B. Zhang, M. Seaberg, D. Popmintchev, M. M. Murnane, and H. C. Kapteyn, "Bright, coherent, ultrafast soft X-ray harmonics spanning the water window from a tabletop light source," Phys. Rev. Lett. **105**, 173901 (2010).
17. T. Popmintchev, M.-C. Chen, D. Popmintchev, P. Arpin, S. Brown, S. Ališauskas, G. Andriukaitis, T. Balčiunas, O. D. Mücke, A. Pugzlys, A. Baltuška, B. Shim, S. E. Schrauth, A. Gaeta, C. Hernandez-Garcia, L. Plaja, A. Becker, A. Jaron-Becker, M. M. Murnane, and H. C. Kapteyn, "Bright coherent ultrahigh harmonics in the keV X-ray regime from mid-infrared femtosecond lasers," Science **336**, 1287–1291 (2012).
18. E. J. Takahashi, T. Kanai, K. L. Ishikawa, Y. Nabekawa, and K. Midorikawa, "Coherent water window x-ray generation by phase-matched high-order harmonic generation in neutral media," Phys. Rev. Lett. **101**, 253901 (2008).
19. A. D. Shiner, B. Schmidt, C. Trallero-Herrero, H. J. Wörner, S. Patchkovskii, P. B. Corkum, J.-C. Kieffer, F. Légaré, and D. M. Villeneuve, "Probing collective multi-electron dynamics in xenon with high-harmonic spectroscopy," Nat. Phys. **7**, 464–467 (2011).
20. N. Ishii, K. Kaneshima, K. Kitano, T. Kanai, S. Watanabe, and J. Itatani, "Carrier-envelope phase-dependent high harmonic generation in the water window using few-cycle infrared pulses," Nat. Commun. **5**, 3331 (2014).
21. S. L. Cousin, F. Silva, S. Teichmann, M. Hemmer, B. Buades, and J. Biegert, "High-flux table-top soft X-ray source driven by sub-2-cycle, CEP stable, 1.85-μm 1-kHz pulses for carbon K-edge spectroscopy," Opt. Lett. **39**, 5383–5386 (2014).
22. A. Johnson, L. Miseikis, D. Wood, D. Austin, C. Brahms, S. Jarosch, C. Strüber, P. Ye, and J. Marangos, "Measurement of sulfur l2, $3L_{2,3}$ and carbon K-edge Xanes in a polythiophene film using a high-harmonic supercontinuum," Structural Dynamics **3**, 062603 (2016).
23. B. E. Schmidt, P. Béjot, M. Giguere, A. D. Shiner, C. Trallero-Herrero, E. Bisson, J. Kasparian, J.-P. Wolf, D. M. Villeneuve, J.-C. Kieffer, P. B. Corkum, and F. Légaré, "Compression of 1.8 μm laser pulses to sub-two optical cycles with bulk material," Appl. Phys. Lett. **96**, 121109 (2010).
24. B. E. Schmidt, A. D. Shiner, P. Lassonde, J.-C. Kieffer, P. B. Corkum, D. M. Villeneuve, and F. Légaré, "CEP stable 1.6 cycle laser pulses at 1.8 μm," Opt. Express **19**, 6858–6864 (2011).
25. G. J. Stein, P. D. Keathley, P. Krogen, H. Liang, J. P. Siqueira, C.-L. Chang, C.-J. Lai, K.-H. Hong, G. M. Laurent, and F. X. Kärtner, "Water-window soft X-ray high-harmonic generation up to the nitrogen K-edge driven by a kHz, 2.1 μm OPCPA source," Journal of Physics B: Atomic, Molecular and Optical Physics **49**, 155601 (2016).
26. D. R. Austin, T. Witting, S. J. Weber, P. Ye, T. Siegel, P. Matía-Hernando, A. S. Johnson, J. W. Tisch, and J. P. Marangos, "Spatio-temporal characterization of intense few-cycle 2 μm pulses," Opt. Express **24**, 24786–24798 (2016).
27. G. Fan, T. Balčiūnas, T. Kanai, T. Flöry, G. Andriukaitis, B. E. Schmidt, F. Légaré, and A. Baltuška, "Hollow-core-waveguide compression of multi-millijoule CEP-stable 3.2 μm pulses," Optica **3**, 1308–1311 (2016).
28. S. M. Teichmann, F. Silva, S. L. Cousin, M. Hemmer, and J. Biegert, "0.5-keV soft X-ray attosecond continua," Nat. Commun. **7**, 11493 (2016).
29. F. Silva, S. M. Teichmann, S. L. Cousin, M. Hemmer, and J. Biegert, "Spatiotemporal isolation of attosecond soft X-ray pulses in the water window," Nat. Commun. **6**, 6611 (2015).
30. N. Saito, N. Ishii, T. Kanai, S. Watanabe, and J. Itatani, "Attosecond streaking measurement of extreme ultraviolet pulses using a long-wavelength electric field," Sci. Rep. **6**, 35594 (2016).
31. Y. Mairesse and F. Quéré, "Frequency-resolved optical gating for complete reconstruction of attosecond bursts,"

Optics EXPRESS

Physical Review A - Atomic, Molecular, and Optical Physics **71**, 1–4 (2005).
32. J. Gagnon, E. Goulielmakis, and V. S. Yakovlev, "The accurate FROG characterization of attosecond pulses from streaking measurements," Appl. Phys. B **92**, 25–32 (2008).
33. M. Chini, S. Gilbertson, S. D. Khan, and Z. Chang, "Characterizing ultrabroadband attosecond lasers," Opt. Express **18**, 13006 (2010).
34. G. Laurent, W. Cao, I. Ben-Itzhak, and C. L. Cocke, "Attosecond pulse characterization," Opt. Express **21**, 16914 (2013).
35. P. D. Keathley, S. Bhardwaj, J. Moses, G. Laurent, and F. X. Kärtner, "Volkov-transform generalized projection algorithm for attosecond pulse characterization," New J. Phys. **18**, 073009 (2016).
36. G. G. Paulus, F. Grasbon, H. Walther, P. Villoresi, M. Nisoli, S. Stagira, E. Priori, and S. De Silvestri, "Absolute-phase phenomena in photoionization with few-cycle laser pulses," Nature **414**, 182–184 (2001).
37. H. Li, N. G. Kling, T. Gaumnitz, C. Burger, R. Siemering, J. Schötz, Q. Liu, L. Ban, Y. Pertot, J. Wu, A. M. Azzeer, R. de Vivie-Riedle, H. J. Wörner, and M. F. Kling, "Sub-cycle steering of the deprotonation of acetylene by intense few-cycle mid-infrared laser fields," Opt. Express **25**, 14192 (2017).
38. T. Carroll, J. Bozek, E. Kukk, V. Myrseth, L. Sæthre, T. Thomas, and K. Wiesner, "Xenon $N_{4,5}$OO Auger spectrum–a useful calibration source," J. Electron. Spectrosc. Relat. Phenom. **125**, 127–132 (2002).
39. M. Huppert, I. Jordan, and H. J. Wörner, "Attosecond beamline with actively stabilized and spatially separated beam paths," Rev. Sci. Instrum. **86**, 123106 (2015).
40. A. S. Kheifets, "Time delay in valence-shell photoionization of noble-gas atoms," Phys. Rev. A **87**, 063404 (2013).
41. J. B. West, and G. V. Marr, "The absolute photoionization cross sections of helium, neon, argon and krypton in the extreme vacuum ultraviolet region of the spectrum," Proceedings of the Royal Society A: Mathematical, Physical and Engineering Sciences, **349**, 397–421 (1976).
42. Jie Li, Xiaoming Ren, Yanchun Yin, Kun Zhao, Andrew Chew, Yan Cheng, Eric Cunningham, Yang Wang, Shuyuan Hu, Yi Wu, Michael Chini, and Zenghu Chang, "53-attosecond X-ray pulses reach the carbon K-edge," Nat. Commun. **8**, 186 (2017).

1. Introduction

Attosecond science is evolving from the study of atoms and small molecules to that of increasingly complex systems and condensed matter. The detailed understanding of the valence-shell spectroscopy of simple molecules has been an essential prerequisite for both the planning and the interpretation of attosecond time-resolved measurements [1–3]. Similar knowledge is, however, not available for larger molecules or condensed-phase systems. In frequency-domain spectroscopy, most work on complex systems is therefore done in the X-ray domain [4]. Transitions in the X-ray spectral region are element specific, sensitive to the chemical environment, the spin state and the oxidation state of the probed element. Transient X-ray spectroscopy therefore offers the potential of obtaining atomically-resolved information on electron dynamics in all phases of matter [5]. Very recently, the first femtosecond time-resolved experiments with a table-top light source at the carbon K-edge have demonstrated the potential of such measurements [6].

The first 15 years of attosecond science have been driven by titanium:sapphire lasers, the initial enabling technology [7–13]. Over the last decade, the development of high-energy sources of longer-wavelength radiation has launched a revolution in attosecond science [14–16], supported by two key aspects. First, the quadratic scaling of the ponderomotive energy with wavelength enables higher photon energies to be generated. This aspect has been extensively demonstrated with continuous coverage of the photon energy range up to 1.6 keV [17–22]. Second, the generation of long-wavelength radiation through either white-light-seeded parametric amplification or intraband difference-frequency generation provides sources of passively CEP-stable radiation [15, 23–27]. This aspect has raised considerable expectations towards the generation of isolated attosecond pulses from such drivers. First evidence consistent with the production of isolated attosecond pulses has been obtained from the dependence of high-harmonic spectra on the carrier-envelope phase [20, 28] and the attosecond lighthouse [29]. Recently, the first streaking experiment with attosecond pulses centered around 95 eV has been demonstrated with a mid-IR OPCPA system [30]. Due to the narrow bandwidth of ≈ 5 eV the attosecond pulse could be reconstructed with the traditionally used algorithms based on frequency-resolved optical gating (FROG) [31,32], which provided a pulse duration of ≈ 450 as.

Optics EXPRESS

The extremely broad energy bandwidth available from mid-IR driven attosecond pulse generation naturally suggests the possibility to synthesize much shorter pulses than previously available. The main obstacle towards this goal is the lack of a general technique for the temporal characterization of SXR supercontinua. The predominant methods fall in two classes. The first class of techniques relies on FROG-type algorithms, such as the principle-component generalized projection algorithm (PCGPA) and the least-squares generalized projection algorithm (LSGPA) [31, 32]. This class of techniques sets stringent limitations on the bandwidth of the attosecond pulses that can be reconstructed because it requires the central-momentum approximation to be made and does not allow for an energy dependence of the photoionization matrix elements. Another class of methods relies on the PROOF approach (phase retrieval by omega oscillation filtering) [33, 34]. The PROOF algorithm relies on the assumption that the streaking effect can be described as a single-photon interaction with the IR field, which is usually not the case. The stability of the PROOF algorithm also strongly relies on a frequency analysis of the streaking spectrogram and is therefore most suitable for multi-cycle IR pulses. Finally, it does not allow for a reconstruction of the IR pulse, removing one important opportunity to cross-check the reliability of the reconstruction.

In this article, we solve the long-standing problem of the temporal characterization of SXR supercontinua by introducing and experimentally demonstrating a general method that overcomes the key limitations of previous attosecond pulse characterization methods. We generalize the recently proposed VTGPA method [35] to the case of multiple overlapping photoelectron bands, thereby making it suitable for SXR supercontinua. The key advantages of this new method (multi-line VTGPA, ML-VTGPA) compared to previous approaches are that (i) the CMA is completely avoided, (ii) the physical, complex-valued, energy-dependent photoionization matrix elements (PMEs) of the target are incorporated and (iii) any target can be used for streaking, provided that the PMEs are available and that the cross sections are suitable. The most important consequence of these advantages is the applicability of this method to attosecond supercontinua of arbitrary bandwidths. We experimentally demonstrate this technique through the synthesis of an isolated attosecond pulse generated from a two-cycle mid-IR pulse through amplitude gating and a complete temporal characterization of both the SXR and mid-IR pulse through attosecond streaking using ML-VTGPA. The retrieved pulse duration of (43±1)as defines a new record of the shortest pulse ever measured.

2. Experiment

2.1. Few-cycle mid-IR pulse generation

Femtosecond laser pulses centered at 800 nm are produced using a Ti:Sa laser system (Femtolasers Rainbow CEP4 + Femtopower PRO V CEP delivering 5 mJ at 1 kHz, 25 fs). The beam is sent to an optical parametric amplifier (Light Conversion, TOPAS HE, conversion efficiency 34 %), to generate 900 μJ pulses centered at 1.8 μm with a pulse duration of 30 − 40 fs. These pulses are subsequently spectrally broadened in a static-pressure hollow-core fiber filled with argon (≈ 1.5 bar) to an octave-spanning spectrum (Fig. 1(a)) with pulse energies up to 480 μJ. Recompression to the few-cycle regime is performed by a pair of fused-silica wedges [23, 24]. The spectrum of the mid-IR pulses is measured with a mid-IR spectrometer (APE WaveScan), and shown in Fig. 1(a), ranging from 1.1 to 2.2 μm. Within the attosecond community, this spectral domain is designated as “mid-infrared”, whereas the term “short-wavelength infrared” is more widely used. The pulse duration is characterized in the optical domain using a home-built transient-grating FROG (TG-FROG), where the reconstruction is performed using a commercial FROG retrieval algorithm (cf. Fig. 1(b), Femtosoft FROG). The reconstructed pulse duration is $\tau_{\mathrm{rec}} = (11.5 \pm 0.8)$ fs and the Fourier-transform limit (FTL) is $\tau_{\mathrm{FTL}} = 7.9$ fs. The CEP stability was independently verified by sending pulses attenuated to 340 μJ into a single-shot stereo-ATI phase meter [36, 37]. The passive CEP stability of the two-cycle mid-IR pulses was found to be

Optics EXPRESS

better than 300 mrad (rms) from a single-shot measurement performed over 30 minutes.

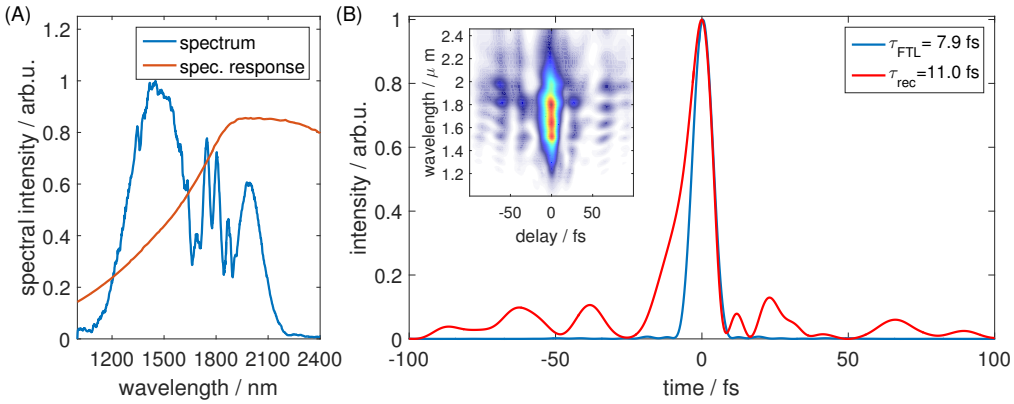

Fig. 1. **Spectrum of the mid-IR pulse and TG-FROG measurement.** A) Typical spectrum of our mid-IR pulses after broadening in the hollow-core fiber (blue) and correction for the spectrometer response (orange). B) Fourier-transform-limited pulse duration calculated from (A) (blue) and reconstructed electric-field envelope from a TG-FROG measurement (red). An exemplary retrieved FROG trace is shown as an inset. Eleven reconstructions have been performed leading to a pulse duration of $\tau_{\mathrm{rec}} = (11.5 \pm 0.8)$ fs, with a FROG error of $(6.8 \pm 1.6) \cdot 10^{-3}$ for the reconstruction.

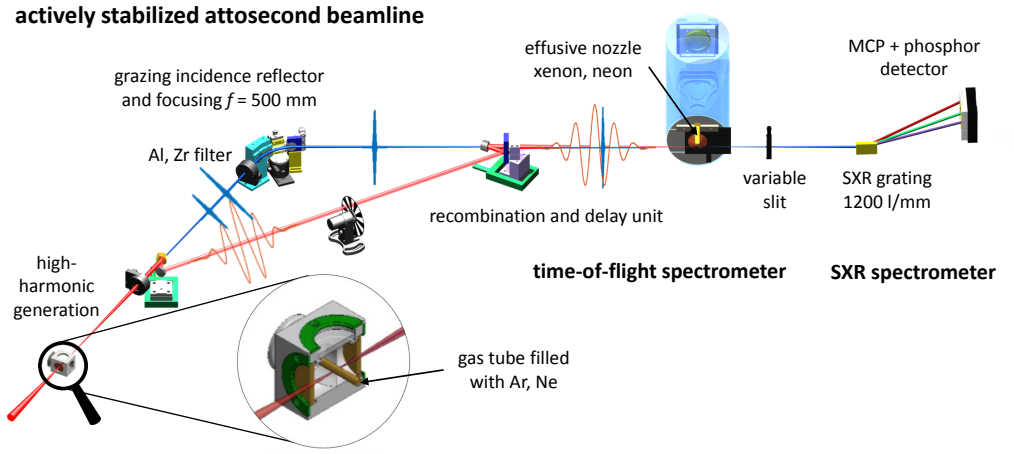

Fig. 2. **Experimental realization of the attosecond streak camera with a mid-IR driver.** Isolated attosecond pulses are created through high-harmonic generation in a high-pressure gas cell filled with neon or argon. The residual mid-IR pulse is separated from the attosecond soft-X-ray pulse by means of a perforated mirror. Broadband reflection of the SXR supercontinuum is achieved through grazing-incidence reflection on 3 flat mirrors coated with diamond-like carbon and one gold-coated toroidal mirror (The calculated overall reflectivity curve is presented in Fig. 3(a) black line.) that focuses the SXR beam into the interaction region of a photoelectron time-of-flight spectrometer. A 100-nm Zr foil acts as a high-pass filter and simultaneously compensates the attochirp. Recombination of mid-IR and SXR pulses is achieved with another perforated mirror that focuses the mid-IR beam to the same spot.

Optics EXPRESS

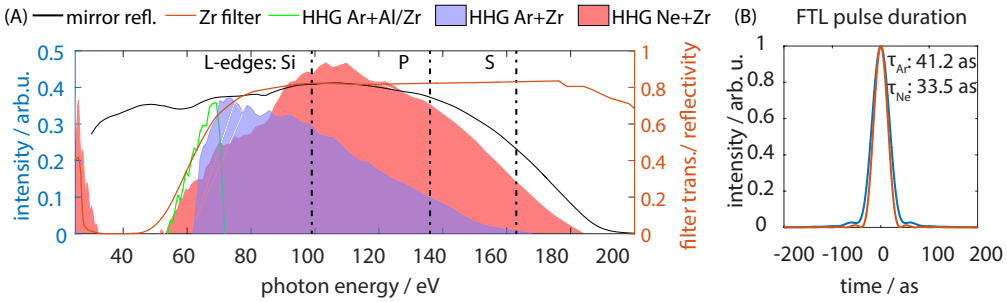

Fig. 3. **Experimental HHG spectra and corresponding Fourier-transform-limited pulses.** A) SXR supercontinua generated in Ar (blue) or Ne (red) detected with a home-built flat-field SXR spectrometer. HHG spectrum with aluminum-zirconium filter stack for calibration (green). B) Intensity profile of the corresponding Fourier-transform limited pulses from the spectra in (A) and the FTL pulse duration.

2.2. *Attosecond streak-camera setup*

Figure 2 shows our experimental setup featuring several unique characteristics. Soft-X-ray supercontinua are generated by focusing two-cycle mid-IR pulses with an off-axis parabolic (OAP) mirror (f = 25 cm, not shown) into a differentially pumped high-pressure gas cell containing neon (900 mbar) or argon (300 mbar). The SXR radiation is separated from the residual mid-IR by a perforated OAP mirror. The SXR beam is reflected on three grazing-incidence mirrors and focused by a toroidal mirror into the interaction region of a photoelectron time-of-flight spectrometer. This 4-mirror system achieves an unusually broad reflectivity as shown in Fig. 3(a) (black curve). The mid-IR beam is recollimated by the same perforated OAP mirror, traverses a chopper which blocks every other mid-IR pulse for single-shot signal referencing and is recombined with the SXR beam by means of a second perforated OAP mirror which simultaneously focuses the mid-IR beam into the interaction region.

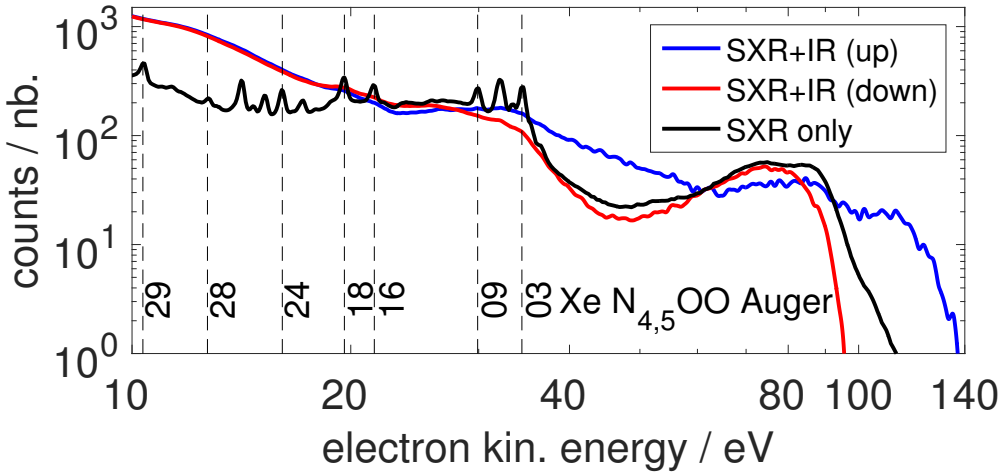

Fig. 4. **Xenon photoelectron spectrum.** Photoelectron spectra recorded by ionizing Xe atoms with an isolated attosecond pulse generated in argon without (black) and with streaking field (blue/red). Auger-electron lines are labeled according to [38].

Optics EXPRESS

The compact design of this beamline achieves a passive temporal stability of ~ 200 as, which is improved to ~ 26 as rms over ≈ 1.5 h by an active multi-color feedback stabilization described in [39]. A photoelectron spectrum obtained by ionizing xenon with an attosecond pulse generated in argon is shown as black line in Fig. 4. The Auger electrons emitted from xenon were used for energy calibration of the electron time-of-flight spectrometer. The photoelectron spectra recorded in the presence of the mid-IR streaking field are also shown for two selected SXR-mid-IR delays corresponding to streaking to higher kinetic energies (blue) or lower energies (red).

The SXR spectra are recorded with a home-built spectrometer consisting of a flat-field grating (Shimadzu, 1200 l/mm) and a MCP+phosphor detector imaged onto a CCD camera (PCO Sensicam) with an integration time of ≈ 500 ms (500 laser shots). An aluminum-zirconium filter stack (each 100 nm) is used for the energy calibration of the photon spectrometer. The SXR pulse generation has been optimized with respect to the photoelectron and photon spectra, mainly with respect to the highest count rate in the photoelectron spectra. A 100-nm Zr foil acts as a high-pass filter and simultaneously compensates the attochirp. The obtained SXR supercontinua generated in argon or neon are shown in Fig. 3(a), while in Fig. 3(b) the corresponding Fourier-transform-limited pulses are presented. Assuming a perfectly compensated attochirp, the generated SXR supercontinua correspond to pulse durations of 41 as and 34 as for generation in Ar and Ne, respectively.

Figure 5(a) shows the effect of the CEP and the mid-IR pulse duration on SXR continua generated in argon. These data were recorded by tuning the amount of fused silica introduced by a pair of wedges, which simultaneously scans the CEP and the duration of the mid-IR pulses. All data reported in this article have been recorded without any feedback stabilization of the CEP. The high contrast of the fringes shown in Fig. 5(a) demonstrates the few-cycle nature and an excellent passive CEP stability of our mid-IR pulses, confirming the results of the stereo-ATI measurement described in subsection 2.1.

The streaking spectrogram is recorded by scanning the SXR-mid-IR delay over a range of ≈ 35 fs in steps of 100 as where the time-of-flight signal for each delay step is integrated over 10 s. A full streaking spectrogram is recorded within ≈ 1 h. Figure 5(b) shows the streaking spectrogram obtained by high-harmonic generation in argon, followed by a 100-nm Zr filter to compensate the attochirp and detecting photoelectrons emitted from xenon. It is dominated by photoelectrons from the 5p and 5s shells that constitute the band at the highest kinetic energies. The second band, centered around 30 eV, consists of electrons from the 4d shell and Auger electrons that are assigned in Fig. 4. Both bands display well-developed streaking traces with streaking amplitudes reaching more than 40 eV in the upper band. The amplitude of the streaking effect clearly decreases from the 5p/5s to the 4d bands, as expected. The very high contrast of the streaking traces immediately establishes the creation of an extremely-well isolated attosecond pulse.

3. Attosecond pulse reconstruction

The temporal characterization of ultra-broadband attosecond supercontinua (≫ 10 eV) remained an unsolved problem up to now. The traditional FROG-type algorithms all require the CMA to be made, an approximation that fails for large spectral bandwidths. Additionally, it becomes essential to include the photon-energy dependence of the photoionization matrix elements (PMEs) of the target for the pulse characterization. A natural target choice for streaking broadband pulses is helium, which possesses a single dominant photoemission line and a flat cross section over a large energy range. However, other targets like neon, krypton or xenon are more favorable because they have higher photoionization cross sections in the soft-X-ray domain. Specifically, at a photon energy of 100 eV the cross sections of xenon (5p) and helium (1s) amount to 1.095 Mb [40] and 0.454 Mb [41], respectively. Depending on the choice of the target, the spectral amplitude and phase and therefore the temporal shape of the photoelectron wave packet can be strongly

Optics EXPRESS

modified as compared to the attosecond pulse, which has to be taken into account in any reliable reconstruction method.

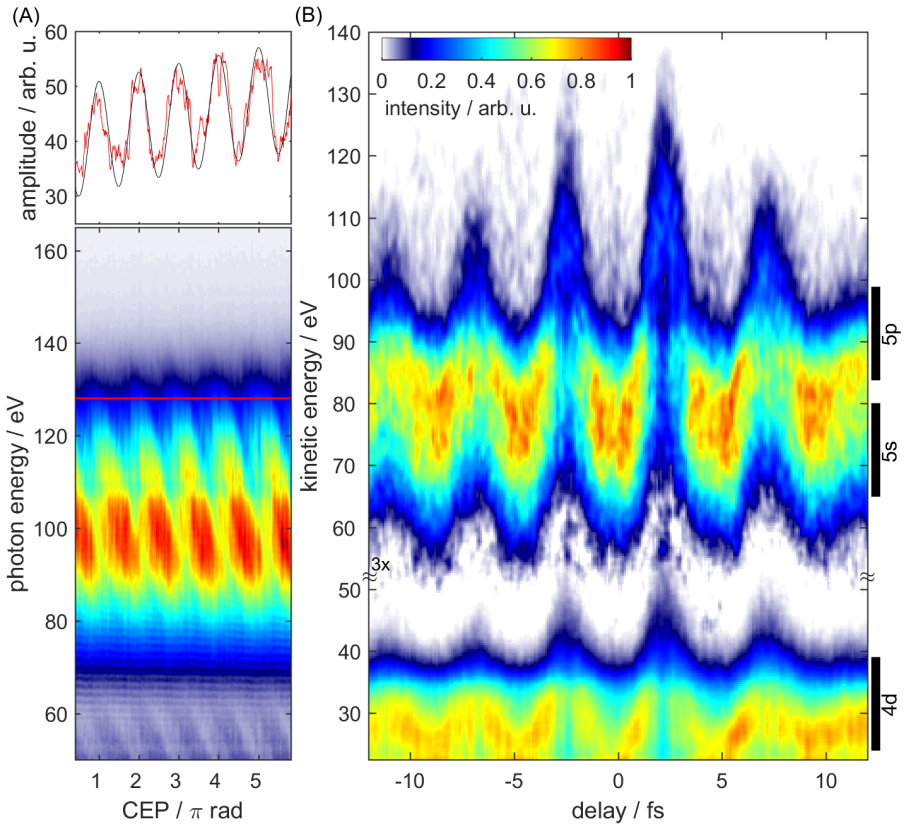

Fig. 5. **CEP dependence of SXR supercontinua and attosecond streaking trace.** A) CEP scan of SXR continua generated in argon and transmitted through a 100-nm Zr filter. A controlled variation of the CEP and pulse duration is achieved by scanning a pair of fused-silica wedges, which translates to a modulation of the shape and cut-off of the SXR continuum. B) Photoelectron streaking spectrogram obtained by ionizing xenon with an attosecond pulse generated in argon by varying the delay between the SXR and mid-IR pulses. The data consists of 350 spectra recorded with a step size of 100 as.

Recently, the Volkov-transform generalized projection algorithm (VTGPA, [35]) has been proposed, which avoids the use of Fourier transformations, circumvents the CMA and therefore enables the incorporation of the target-atom PMEs. The VTGPA has been tested with experimental data in the regime of attosecond pulse trains and with numerical simulations of isolated attosecond pulses. It has been shown to faithfully retrieve attosecond pulses with complex temporal structures and broad spectral bandwidths. VTGPA has been shown to systematically retrieve the correct attosecond pulse duration, in contrast to the tendency of LSGPA to underestimate this quantity. In its original formulation, the VTGPA is limited to spectrograms consisting of a single photoelectron band. Here, we adapt this formulation to include multiple overlapping photoelectron bands. Due to the very large bandwidths of our SXR pulses, photoelectrons measured at a given energy may originate from different initial electronic shells, which have been ionized to the

Optics EXPRESS

same final photoelectron energy by different frequencies within the attosecond pulse bandwidth. The measured spectrogram is then the incoherent sum of several energy-shifted streaking spectrograms, which differ from one another because of the different PMEs. The individual streaking spectrograms are added incoherently because each of them corresponds to leaving the cation in a different final eigenstate, such that quantum-mechanical interference is forbidden. To achieve an accurate reconstruction, multiple photoelectron bands, each with its own PMEs, have to be incorporated simultaneously in the reconstruction. For this purpose, we have implemented the ML-VTGPA.

Within the ML-VTGPA, the complete streaking spectrogram is interpreted as a superposition of streaking spectrograms resulting from M individual photoelectron bands

$$S(p,\tau) = \sum_{i=1}^{M} S_i(p,\tau), \tag{1}$$

generated from a SXR pulse with envelope $\tilde{E}_{\mathrm{XUV}}(t)$ and a mid-IR pulse described by the vector potential $A(t)$. The vector potential $A(t) = A_0^{(N)}(t)\cos\alpha(t)$ is represented by expanding its phase into a power series $\alpha(t) = \alpha_0 + \alpha_1 t + \alpha_2 t^2 + \alpha_3 t^3 + ... + \alpha_k t^k$, where α_0 is the absolute phase, α_1 is the carrier frequency, and the higher order coefficients α_2,...., α_k represent the chirp of the mid-IR pulse. The field envelope $A_0^{(N)}(t)$ is described by a cubic spline interpolation of a set of N supporting points. The streaking spectrogram $S_i(p,\tau)$ at momentum p and relative time delay τ between SXR and mid-IR pulses corresponding to a photoelectron band with ionization potential $I_{\mathrm{p},i}$ is calculated by numerical integration of the following expression, which derives from the strong-field approximation, but includes the proper, accurate PMEs $d_i(p)$:

$$\begin{aligned} S_i(p,\tau) &= \left| \int_{-\infty}^{\infty} \tilde{E}_{\mathrm{XUV}}(t-\tau) d_i(p+A(t)) e^{-i\phi(p,t)} e^{i(p^2/2+I_{\mathrm{p},i})t}\,\mathrm{d}t \right|^2 \\ \phi(p,t) &= \int_t^{\infty} \left(pA(t') + A^2(t')/2 \right) \mathrm{d}t'. \end{aligned} \tag{2}$$

The intensities and the Wigner time delays of the individual photoelectron bands ($i = 1, ..., M$) are fully taken into account through the photon-energy dependent complex-valued PMEs $d^{(i)}(p)$.

The iterative algorithm, illustrated in Fig. 6(b), is initiated with many different initial starting guesses for $\tilde{E}_{\mathrm{XUV}}(t)$ and $A(t)$ to test the stability of the reconstruction. The SXR and mid-IR pulses for the next iteration of the algorithm are then calculated by minimizing the error between the measured spectrogram $S'(p,\tau)$ and the spectrogram $S(p,\tau)$ calculated on the basis of the input SXR and mid-IR pulses on the basis of Eq. (2). The minimization of the error is performed by using the least-squares method for the SXR pulse and Brent's method for the mid-IR pulse. These different error-minimization methods were chosen because of their specific efficiencies with respect to the chosen functional forms of the SXR and mid-IR pulses.

In our experimental reconstruction (see section 4), we use the PMEs of the 5p and 5s shells of xenon [40], calculated by the the random-phase approximation (RPA). This theoretical method represents the state of the art in atomic photoionization and takes both independent-electron and inter-shell correlation effects into account. In the case of the 5s electrons, only one transition from the bound to the continuum is possible (5s→Ep), while for the 5p electrons two transition pathways have to be taken into account (5p→Ed and 5p→Es).

4. Results and discussion

Before analysis with the ML-VTGPA, all spectrograms are converted to the energy domain and Jacobi corrected. A center-of-energy analysis of the spectrogram is applied to separate the

Optics EXPRESS

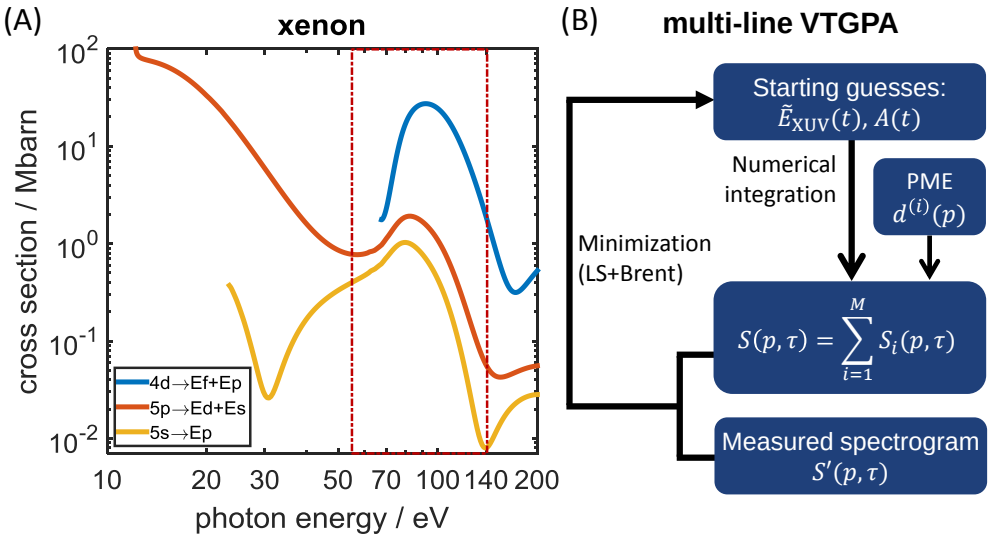

Fig. 6. **Photoionization cross sections of xenon and multi-line VTGPA flow chart.** A) Cross section for xenon 4d, 5s, and 5p photoelectron bands [40], SXR photon energy region (red box). B) Flow chart of the ML-VTGPA method. Initial guesses for $\tilde{E}_{\mathrm{XUV}}(t)$ and the mid-IR vector potential $A(t)$ enter the iterative algorithm which consists of numerical integration of equations (1) and (2) using the PMEs $d^{(i)}(p)$. The errors are minimized with least-squares and Brent's method for the SXR and mid-IR pulses, respectively, before the new guesses are fed into the next iteration of the algorithm.

overlapping 5p/5s photoelectron bands at high kinetic energies from the 4d/Auger lines at lower kinetic energies (see Fig. 5(b)).

For our reconstruction, we concentrate on the region of the spectrum containing contributions from the 5p and 5s shells of xenon. This part of the spectrum is clearly separated from the 4d and Auger electrons and displays the largest streaking amplitude because of the high kinetic energy of the photoelectrons. This spectral region therefore ideally lends itself to the reconstruction of the SXR attosecond pulse. Figure 7(a) shows the selected high-energy part of a streaking spectrogram, recorded under conditions similar to Fig. 5(b). We note that the rapid decay of the 5p and 5s photoionization cross sections of xenon beyond ~ 100 eV (Fig. 6(a)) causes an apparent drop of the photon spectrum in this energy range. This effect is naturally included in our ML-VTGPA method and has no detrimental effect on the reconstruction.

The center-of-energy analysis of the streaking spectrogram is also used to generate an initial guess for the vector potential of the mid-IR pulse. More precisely, the phase $\alpha(t)$ is expanded in a fourth-order polynomial, i.e. taking second- and third-order chirp into account, as described in section 3. The electric-field envelope $A_0^{(N)}(t)$ is represented by $N = 13$ equidistant supporting points connected by a cubic-spline interpolation, with an initial guess obtained from the Hilbert transform of the center of energy of the streaking trace. The initial guess of the SXR pulse envelope is represented by a Gaussian of variable width. The reconstructed streaking spectrogram combined with the retrieved scaled vector potential of the mid-IR pulse are shown in Fig. 7(b). The streaking spectrogram is reproduced with high fidelity. The reconstructed attosecond pulse has a FWHM duration of $\tau_{\mathrm{SXR}} = (43 \pm 1)$ as and displays an excellent contrast as shown in Fig. 7(c). The electric field of the retrieved mid-IR pulse is shown in Fig. 7(d) together with the electric-field envelope and the Fourier transform of the measured mid-IR spectrum (cf. Fig. 1). The retrieved mid-IR pulse (blue and black lines) has an envelope duration of $\tau_{\mathrm{mid-IR}} = (11.1 \pm 0.7)$ fs, which is in very good agreement with our TG-FROG measurement $\tau_{\mathrm{rec}} = (11.5 \pm 0.8)$ fs (green dotted

Optics EXPRESS

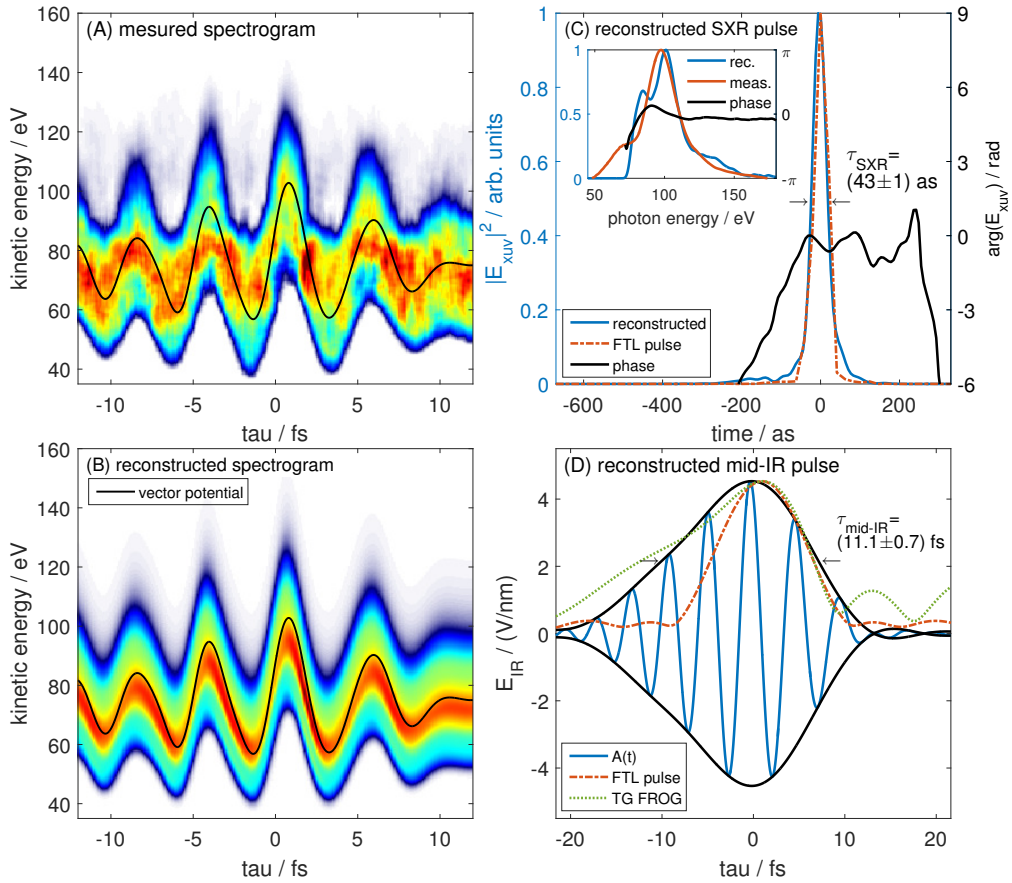

Fig. 7. **Analysis of streaking spectrogram and reconstructed attosecond pulse.** A) Measured attosecond streaking trace obtained in xenon and B) Retrieved spectrogram with scaled mid-IR vector potential obtained using the ML-VTGPA algorithm. C) Temporal amplitude (blue) and phase (black) of the isolated attosecond pulse. The reconstruction by our ML-VTGPA algorithm provides an SXR pulse duration of $\tau_{\mathrm{SXR}} = (43 \pm 1)$ as and a mid-IR pulse duration of $\tau_{\mathrm{mid-IR}} = (11.1 \pm 0.7)$ fs. The merit was found to be $4.3 \cdot 10^{-3}$. The Fourier-transform-limited pulse (dashed red) calculated from the SXR photon spectrum measured in parallel to the streaking experiment. Measured (red) and reconstructed (blue) spectra with the reconstructed spectral phase (black) of the attosecond pulse are presented in the inset. D) The vector potential of the mid-IR pulse obtained from the VTGPA reconstruction in comparison with the Fourier-transform-limited pulse (dashed red) calculated from the measured spectrum shown in Fig. 1(a) and the pulse measured with our home-built TG-FROG (dotted green).

line), although the detailed shapes of the two pulses differ somewhat. The Fourier-transformed mid-IR spectrum (red dash-dotted line) demonstrates that the mid-IR pulse (black) is reasonably close to the Fourier limit.

We have verified the stability of the reconstruction by changing the initial guess for the mid-IR pulse in carrier frequency, absolute phase and vector-potential envelope $A(t)$, as well as the initial pulse duration of the SXR pulse. A total of three independent streaking spectrograms were analyzed. In each case, multiple sets of input parameters were used and all obtrained results entered the statistical analysis. The quoted pulse duration refers to the average of eight reconstructions obtained in this way and the error interval corresponds to the standard deviation of the pulse

Optics EXPRESS

duration. This systematic study confirms the robustness of the ML-VTGPA reconstruction of our SXR attosecond and mid-IR two-cycle pulses. The additional agreement between the ML-VTGPA and the fully independent TG-FROG reconstructions of the mid-IR pulse further corroborates the reliability of our reconstruction.

5. Conclusion and outlook

We have demonstrated the scalability of attosecond metrology to mid-IR drivers, including both amplitude gating and the attosecond streak camera. This represents an important advance in attosecond science for several reasons.

First, it establishes the popular, robust and widespread scheme for generating CEP-stable two-cycle pulses in the mid-IR [23] as an ideal approach to generating the shortest isolated attosecond pulses ever measured. Our results show that these pulses can come close to being Fourier-transform limited, have a very high contrast and reach the SXR domain. This approach will additionally considerably reduce the technical complexity of attosecond experiments, by removing the need for the active stabilization of the CEP, which might be crucial to their wider application.

Second, our work demonstrates the feasibility of amplitude gating in the ultra-broadband SXR regime. Compared to polarization gating, it offers higher peak intensities for the driving field and optimal conversion efficiencies. It is therefore well suited to achieve high photon energies and high photon fluxes, which are essential for the implementation of X-ray experiments [6].

Third, we have extended the recently proposed VTGPA method to multiple overlapping photoelectron bands and have shown that our ML-VTGPA method is ideally suited for the characterization of ultra-broadband SXR pulses. The ML-VTGPA method overcomes the bandwidth limitations imposed by the central-momentum approximation and includes the complex photoionization matrix elements of the target system used. With this method we have retrieved a new record pulse duration of (43 ± 1) as generated from a two-cycle mid-IR driver laser with a (11.1 ± 0.7) fs pulse duration.

Fourth, since our reconstruction method does not contain any inherent bandwidth limitation and incorporates the target-specific, physical PMEs, this work demonstrates a path towards synthesizing and characterizing attosecond pulses shorter than one atomic unit of time (24 as). Although the bandwidth of the SXR supercontinuum generated in neon (Fig. 3(a)) is limited by the mirror reflectivity, it already possesses a Fourier limit below 34 as, as shown in Fig. 3(b). Comparing this FTL pulse duration with the retrieved pulse duration of (43 ± 1) as, shows that the SXR pulse is also reasonably close to being Fourier-transform limited, which is also reflected in the spectral phase presented in the inset of Fig. 7(c). This shows that the attochirp has been properly compensated over a dominant fraction of the spectral bandwidth.

Finally, our work scales attosecond metrology to the photon-energy range of element-specific core-to-valence transitions. The L-edges of silicon (99 eV), phosphor (136 eV) and sulfur (163 eV) already lie within the energy range covered by our experimental spectra. Further improvements will bring the K-edges of boron (188 eV), carbon (284 eV) and nitrogen (401 eV) within reach. Access to element-specific X-ray transitions will considerably expand the scope of attosecond science and open up a new level of complexity in studies of molecules, solids and liquids with unprecedented time resolution.

Note added: During submission of this manuscript, we have become aware of the publication of Li *et al.* [42], which reports on the streaking of 53-attosecond soft-X-ray pulses and their reconstruction using the PROOF algorithm.

Funding

ERC Starting Grant (contract 307270-ATTOSCOPE); NCCR-MUST, a funding instrument of the Swiss National Science Foundation; SNF (200021_159875).

Optics EXPRESS

Acknowledgments

We thank N.G. Kling and M.F. Kling for providing the stereo-ATI spectrometer used in this work and A. Kheifets for providing the PMEs of xenon in numerical format.